PRAMANA
— journal of
physics

Vol. 68, No. 6
June 2007
pp. 983–994

A high resolution X-ray crystal spectrometer to study electron and heavy-ion impact atomic collisions

AJAY KUMAR, D MISRA, A H KELKAR, U R KADHANE, K V THULASIRAM and LOKESH C TRIBEDI
Tata Institute of Fundamental Research, Colaba, Mumbai 400 005, India
E-mail: lokesh@tifr.res.in

MS received 9 March 2006; revised 9 March 2007; accepted 11 April 2007

Abstract. We have studied fast ion–atom and electron–atom collision processes using a reconditioned high resolution X-ray spectrometer. The X-rays, generated by the collisions, are dispersed by a curved ADP crystal (Johansson geometry) and detected by a gas proportional counter. A self-written LabVIEW based program has been used to give precise and controlled movement to the crystal and for data acquisition. The performance was tested by detecting the Kα diagram and satellite lines of several elements. The Kα satellite lines of Al have been studied in collision with 3–12 keV electrons and 40 MeV C^{4+} ions. In ion collisions as large as four L-vacancies are created simultaneously with the K-vacancy, compared to two satellites in case of the e-impact. In addition, we have measured the X-rays from H-, He- and Li-like Si ions which arise due to the electron loss/capture process in highly charged 80 MeV Si^{7+} ions in collision with thin carbon foil. Approximate charge state distribution has been obtained using this new technique.

Keywords. Crystal spectrometer; X-rays; highly charged ions; electron impact; ionization.

PACS Nos 39.30.+w; 32.30.Rj; 32.70.Jz; 34.50.Dy

1. Introduction

X-ray spectroscopy is an important tool in probing the atomic structure and a crystal spectrometer is most commonly used for this purpose. The wavelength dispersive spectrometer (or crystal spectrometer) works on the Bragg principle and utilizes the property of a single analyzing crystal to separate or disperse the polychromatic beam of photons from the target. In spite of their poor efficiency, these spectrometers have proven their superiority on resolution and therefore have capabilities to resolve complex multiplet structures in the atomic spectra.

Following the first crystal spectrometer built by Bragg [1] using a flat crystal in reflection mode, several types of such spectrometers have been constructed, such as reflection [2,3] and transmission [4,5] type. In order to enhance the intensity of the

diffracted X-rays further, the effective crystal area has to be increased and following conditions should be satisfied simultaneously at all points of the crystal surface [5]: (a) the angles of incidence and reflection in the reflecting atomic planes must be equal (i.e., focusing condition) and (b) the Bragg angle should be equal (Bragg condition). For a particular photon energy, the Bragg condition will be satisfied at a large area of the crystal if the crystal lattice planes are bent on a cylinder having radius equal to the diameter of the Rowland circle, and for focusing condition the crystal lattice planes should be bent on a cylinder having radius equal to the radius of Rowland circle. In Johansson [3] geometry, almost the whole crystal surface contributes to the diffracted X-rays. Details of similar crystal spectrometers can also be found in refs [6,7].

We have reconditioned a crystal spectrometer which was commercially obtained earlier. Several couplings/components including a new crystal were introduced. A self-written PC based program using LabVIEW has been used for automation and data acquisition. However, besides substantial improvement of the spectrometer we have used it in studying various aspects of ion–atom and electron–atom collision physics. For example, we present the satellite structure of Al in collisions with 10 keV electrons as well as 40 MeV C^{4+} ions. This allows one to compare directly the similarities and differences in the ion–atom and electron–atom ionization processes. One can see how the sensitivity of the spectrometer helps in investigating the multiple outer-shell ionization simultaneously with the K-shell ionization. It may be noted that many of the earlier studies on inner shell X-rays employed Si(Li) detectors of resolution of about 160 eV at 5.9 keV. As a result, there was no possibility to resolve the satellite structure. Therefore the average number of L-vacancies simultaneously with K-vacancy was determined by looking into the shift of the K-X-ray peaks and from the intensity ratios of the Kα and Kβ lines. These information were then used to determine the K-shell fluorescence yield which is required for the derivation of the absolute cross-section of the K-shell vacancy formation. With the high resolution X-ray measurements this quantity can be determined from the satellite structure which is a model-independent way. Besides the Al target we have also studied the K-ionization of the K and Cl and the M-shell ionization of Au. In addition to the target ionization we have investigated in detail the ionization of the highly charged projectiles, such as Si^{7+} ions. The different X-ray lines arising from the H-, He- and Li-like ions are well resolved. The present investigation therefore is aimed to explore the single and multiple ionization of (target) atoms and highly charged (projectile) ions besides the performance test of the spectrometer. The design and performance of this crystal spectrometer along with the automation, using the LabVIEW technique, is described in the following sections.

2. Experimental details

The BARC–TIFR pelletron accelerator facility at TIFR has been used to get highly charged C^{4+} and Si^{7+} ions. The well-collimated beam was made to collide with target. Thin elemental targets of C, Al, KCl and Au have been used in the present work. The C (20 μg/cm^2), Al (100 μg/cm^2) and Au (300 μg/cm^2) foils were self-supporting, and KCl (70 μg/cm^2) was evaporated on C (10 μg/cm^2) backing. A

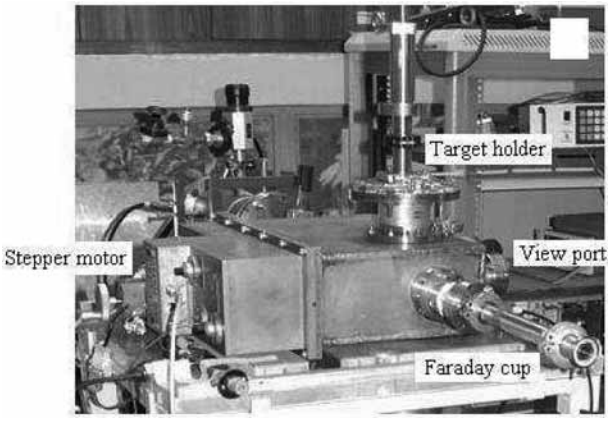

Figure 1. The assembly showing the scattering chamber, beamline components and target holder.

X–Y–Z movable ladder target holder has been used and provision is being made to incorporate a rotatable multiple target holder with 27 targets on a disc. In the present work, we have used ADP (101) ($2d$ = 10.648 Å) crystal in Johansson geometry (in horizontal focusing) [8]. The radius of curvature of the crystal is 12.7 cm and its dimension is $25.4 \times 12.64 \times 0.5$ mm^3. KAP (100) ($2d$ = 26.632 Å) and LiF (200) ($2d$ = 4.027 Å) crystals of similar dimension and radius of curvature have also been procured to cover a wide range of photon energy. Proper choice of the crystal is critical and details of various crystals can be found in [9].

The diffracted X-rays from the crystal are detected by a cylindrical gas proportional counter. A thin polypropylene sheet is placed on the 1 mm wide detector window slit. Negative voltage is given to the detector body by a stabilized power supply and the signal is taken from the anode wire. Detector performance was independently checked using a ^{55}Fe radioisotope. Proportional counter has been operated at 2200 V and P-10 gas (flow mode) pressure was kept typically about one atmosphere. An arrangement has been made for steady gas flow inside the proportional counter using two mechanical leak valves at the inlet and outlet. The gas pressure is measured at the outlet using a digital pressure meter.

The whole assembly of crystal spectrometer is enclosed within a rectangular SS chamber of dimension approximately $40 \times 42 \times 13$ cm^3. The chamber is divided into two parts; the detector and crystal assembly is permanently attached to one part. Feedthroughs for detector high voltage supply, detector output, crystal adjustment, focal circle adjustment, crystal changer and stepper motor are attached to this part of the chamber. Second part of the chamber consists of various other ports (figure 1). A turbomolecular pump is used and typical pressure obtained in the chamber is $\sim 5 \times 10^{-6}$ mbar.

The target is fixed in place, and the crystal and detector both move to change the Bragg angle (by keeping θ–2θ relation) and also remain on the periphery of Rowland circle. The arrangement for movement of crystal and detector is mechanically complex, to maintain the appropriate geometry the crystal rotate on its vertical axis as target-crystal distance changes. The crystal takes translational as well

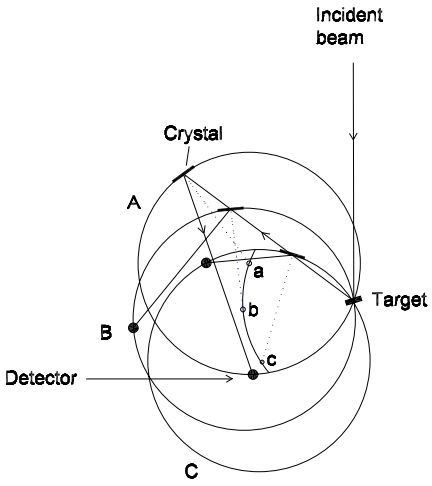

Figure 2. Schematic of movement of the crystal and detector. Open circles a, b and c are the center of the Rowland circle at three given crystal positions.

as rotational motion, and the detector moves on a circular path. The center of Rowland circle also moves on an arc (see figure 2). Typical movement of crystal and detector is shown schematically in figure 2.

The crystal and detector movement is driven by a single stepper motor through high precision tooth wheel mechanism. Two crystals can be mounted at a time on the crystal holder in such a way that one crystal faces the beam and the other sits beside the first crystal but with opposite direction (i.e., back facing the beam). The second crystal comes in the beam path by rotating the holder by 180°. The crystal can be changed from outside, without breaking the chamber's vacuum, through a crystal changer to cover a wide range of photon energy. In the present spectrometer, the photon energy can be scanned between the Bragg angles 12°–70°. One complete rotation of the stepper motor gives typically 0.63 mm linear and 0.15° angular step to the crystal. The scanning resolution depends upon the stepper motor clock. A stepper motor controller has been made, which provides typical minimum linear distance of 1.6 μm and minimum angular step of 1.3″ to the crystal.

The details of the schematic of data acquisition and experimental arrangement are given in figures 3 and 4, respectively. The output signal of the proportional counter is fed to the charge sensitive preamplifier and then to the spectroscopy amplifier. The amplifier output is fed to single channel analyzer (SCA) (figure 4). The incident beam current on the target was measured using an isolated Faraday cup and a current integrator.

2.1 *Stepper motor control and data acquisition*

A stepper motor gives movement to the crystal and detector for scanning an X-ray energy region. Both manual and automatic operation of the stepper motor is provided. For automatic scan, a self-written program based on National Instruments

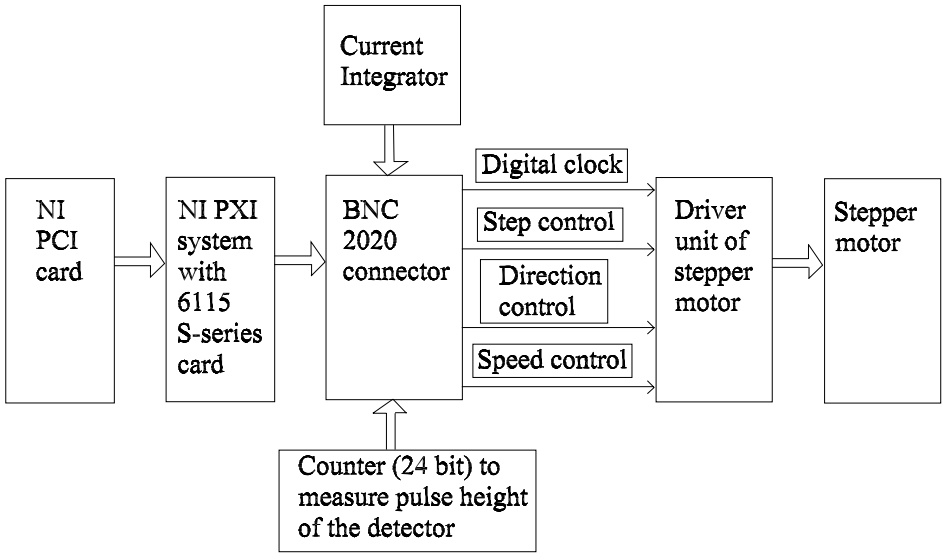

Figure 3. Electronic system configuration of LabVIEW programme.

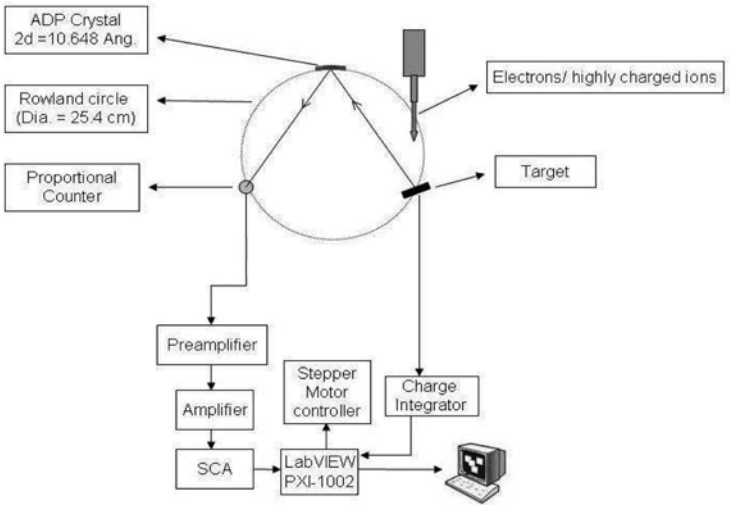

Figure 4. Schematic of the crystal spectrometer set-up.

LabVIEW 6.1 V is being used for stepper motor control and data acquisition. A stepper motor controller is attached between stepper motor and National Instruments NI 6115 module mounted on a PXI 1002 chassis. This chassis accommodates the controller and various I/O modules for control and measurement options.

The stepper motor requires signals to control: (1) direction (2) step size (3) speed and (4) pulse train. All these control signals are derived from the NI 6115 general purpose simultaneous 10 MHz sampling PXI (PCI eXtension for Instrumentation)

module (figure 3). This module contains four analog input channels, two analog output channels, eight digital I/O lines and two counters (24 bits). The counters are used for counting the pulses from current integrator (counter 1) and detector output through single channel analyzer (counter 2). One digital I/O line is used to generate the pulsing clock and three digital I/O lines viz., DI0, DI1, DI2 were used to control: (1) direction, (2) step size and (3) speed of the stepper motor (400 or 200 steps per rotation).

The number of stepper motor rotation ($n_{\rm rot}$) was found to be proportional to the sine of the Bragg angle ($\sin\theta$). The Bragg's equation ($n\lambda = 2d\sin\theta$) and slope of the straight line ($n_{\rm rot}$ vs. $\sin\theta$, not shown here) gives the relation between X-ray energy and stepper motor rotation. Before starting the measurement, the crystal was kept at highest/lowest Bragg angle (extreme positions). The initial and final X-ray energy values of spectrum (to be scanned) are fed in the user interface (UI), which converts it into the number of rotation and in turn the number of pulses required by the stepper motor to scan the given X-ray energy range. First, the stepper motor brings the crystal at the angle of a given starting X-ray energy of the spectrum from the extreme position, without taking the data. From this position, counters 1 and 2 start acquiring the data. When preset value of number of pulses from current integrator (CI, defined in the program) accumulated; both the counters stop counting the pulses. The control digital I/O lines DI0, DI1, DI2 moves the crystal to the next predefined step and re-starts the counters 1 and 2 simultaneously. This process repeats until the final predefined X-ray energy value is reached. Movement of the crystal through the program gives us good reproducibility in its position. At the end of the scan, setup parameters and the complete data is stored in a separate file (ASCII format) for further analysis. Online display panel contains all the setup parameters and live data.

3. Performance

Schematic of the spectrometer set up along with necessary electronics is shown in figure 4. In the crystal spectrometers, alignment of different components (i.e, target, crystal and detector) is critical. All the three components should be horizontally and vertically aligned, and must lie on the periphery of the Rowland circle. A He–Ne laser along with a mirror at the target position was used for precise alignment. The light spot reflected from the mirror will be further reflected by the crystal and should enter in the detector window. This condition must be satisfied at all the crystal position on the rail. For proper alignment, we are having the option of: (1) inward–outward movement of focal plane (to get the target position on the circumference of the Rowland circle), (2) crystal rotation on its vertical axis (to make it tangential on the Rowland circle) and (3) X–Y–Z movement of the target. All this can be done from outside without breaking the chamber's vacuum. Final alignment was done with the target X-rays by checking the count rate at the X-ray peak centroid position.

Proportionality of stepper motor rotation to the incident X-ray wavelength was checked by measuring the angle (i.e., Bragg angle, θ), geometrically, at each 50 rotations interval of the stepper motor. The $\sin\theta$ has been plotted (not shown)

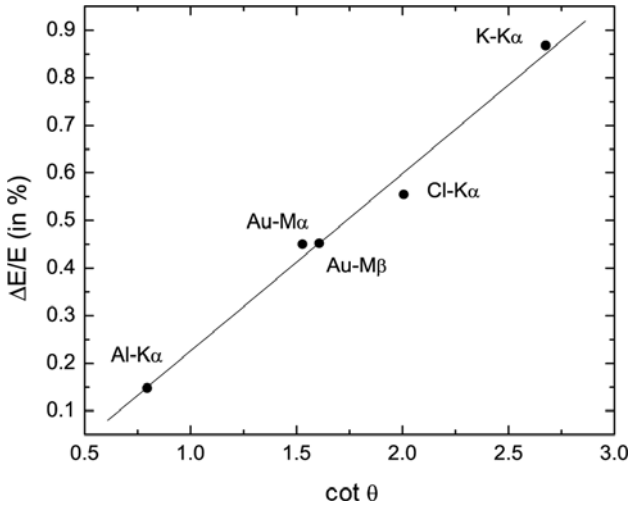

Figure 5. Spectrometer resolution as a function of cot θ.

against the number of stepper motor rotation which is found to be a straight line, as expected. The energy calibration of the spectrometer was done, for the first-order reflection of the ADP crystal, using the X-rays from thin targets of Al, Cl, K and Au excited by electrons [10]. The Bragg angles of the X-ray peak position were found close to the geometrically measured angle. The reproducibility in the X-ray peak position has been found to be ± 1 eV in case of Al and this is due to the backlash in the worm gears.

Three parameters characterize a crystal spectrometer: (a) dispersive power ($\Delta\theta/\Delta\lambda$), (b) spectral resolution or resolving power ($\lambda/\Delta\lambda$ or $\Delta E/E$) and (c) reflecting power or reflectivity of the crystal. The quoted reflectivity of the present ADP crystal is close to one for Al–K X-rays [8]. The dispersive power of the spectrometer has been found to be 0.047°/Å (at 1488 eV) and 0.016°/Å (at 2204 eV). For improving the resolution, either incident beam should be narrow and collimated or X-ray source should be smaller [11]. In order to get the collimated beam of electrons/ions, an Al tube (30 cm long and 2.5 cm diameter) having 4 mm collimator at the target side has been attached to the chamber at the beam entrance. The distance between target-to-beam collimator is about 4 cm. The FWHM of the Al KαL^0 X-ray peak (1488 eV) was found to be 2.7 eV. The $\Delta E/E$ (in %) has been plotted as a function of cot θ in figure 5, where ΔE is the FWHM of the X-ray peak at energy E. From this curve it is clearly seen that for a given crystal, $\Delta E/E$ increases i.e. resolution decreases as X-ray energy increases (or Bragg angle decreases). From eq. (1), $\Delta E/E$ is proportional to cot θ, and therefore resolution improves as angle increases. Bombarda [11] has elucidated on various contributions in the observed peak width and final instrument resolution was shown to be the quadrature sum of all the contributing factors. Cauchios and Bonnelle [12] has also found that crystal width, crystal height, effect of non-vanishing angle between the lattice planes and the crystal surface contributes to the observed broadening in the X-ray peak.

4. Studies on inner shell ionization

4.1 *Al–K-satellite structure: Electron impact*

The Al–K X-ray spectrum taken with 10 keV electrons are presented in figure 6a. The diagram ($K\alpha L^0$) and satellite ($K\alpha L^1$, $K\alpha L^2$) lines of Al were found to be well-separated. The $K\beta$ line can also be seen in the spectrum. The origin of satellite lines is due to multiple ionization in the L shell simultaneously with the ionization in the K shell. For example, the $K\alpha L^1$ satellite corresponds to double inner-shell ionization (single K-ionization along with one L-vacancy) and similarly $K\alpha L^2$ represents triple ionization. The ratio of yields of Al first satellite ($K\alpha L^1$)-to-diagram ($K\alpha L^0$) line was found to be 12.2%, 11.0%, 11.5%, 11.1% and 10.8% for 3, 5, 7, 10 and 12 keV electrons, respectively, which are in close agreement with the values measured by Mauron and Dousse [13] in the present electron energy region. To the best of our knowledge, this is the first observation of the second satellite ($K\alpha L^2$) line of Al with electron impact and the observed intensity of this line is about 1% of the diagram line (i.e. triple-to-single ionization ratio). The ratio of second-to-first satellite X-ray yield gives the information of double-to-single L shell vacancy (simultaneous with K shell) (i.e. triple-to-double ionization of the atom). The $K\alpha$ diagram and up to two satellite lines of Si have been measured in photoionization by Santra *et al* [14] using a curved PET crystal. A multiple Gaussian peak fitting subroutine was used to estimate the peak area. The statistical error in the $K\alpha L^0$, $K\alpha L^1$ and $K\alpha L^2$ peak area evaluation are <1%, <1% and $\sim$ 7%, respectively, and arising due to statistics, fitting procedure and background subtraction.

The Cl- and K- K-X-ray spectrum in collision with 14 keV electrons are presented in figure 6b. In these spectra, only $K\alpha$ diagram line is observed at peak positions 2622 eV and 3310 eV, respectively; which are in close agreement with the theoretical values given in [10]. The satellite lines are not observed (figure 6b) due to lower cross-section of outer shell ionization of K and Cl with respect to Al and also due to the use of higher energy electrons. The third example for the performance of the spectrometer is displayed in figure 6c in which we show the M X-ray spectrum of a thin Au foil bombarded by 14 keV electrons arising from M subshell ionization. The $M\alpha$ (M_5-$N_{6,7}$) and $M\beta$ (M_4-N_6) lines are well resolved, having energies at 2122 eV and 2204.6 eV, respectively. In the same figure we also show $M\alpha\beta$ spectrum taken using Si(Li) detector (160 eV FWHM at 5.89 keV) in collision with 95 MeV F^{8+} ions on thin Au foil. One can clearly see that the Si(Li) detector is not able to resolve the components of M X-ray lines. Further, the heavy ions create multiple vacancies in the higher shells simultaneously with M shell. Therefore, in case of F^{8+} impact the Au $M\alpha\beta$ X-rays comes at the higher energy side compared to that produced by electron impact (figure 6c). To the best of our knowledge, high resolution spectrum of Au M-X ray has not been observed before except a similar spectrum for Th has been reported [15].

4.2 *Al–K-satellite structure: Heavy-ion impact*

The situation changes dramatically when target X-rays are produced in collision with heavy ions. One now observes up to four satellite lines in addition to the

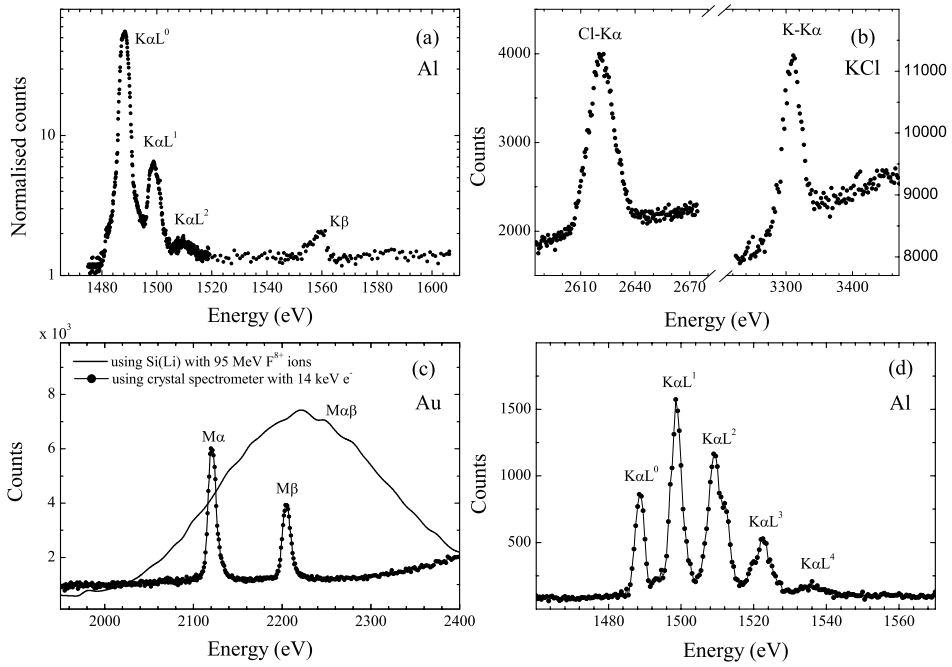

Figure 6. (**a**) Al–K X-ray spectrum with 10 keV electrons showing the diagram line (KαL^0), two satellite lines and also Kβ; (**b**) Cl- and K-Kα X-rays with 14 keV electrons; (**c**) Au-Mα and -Mβ X-rays with 95 MeV F^{8+} ions and 14 keV electrons using Si(Li) and crystal spectrometer, respectively; (**d**) Al Kα X-rays with 40 MeV C^{4+} ions, showing diagram and four satellite lines.

diagram line in ionization of Al target by 40 MeV C^{4+} ions. The diagram (KαL^0) and satellite (KαL^1, KαL^2, KαL^3 and KαL^4) X-ray lines of Al are found to be well-separated (figure 6d). The peak positions of KαL^0, KαL^1, KαL^2, KαL^3 and KαL^4 X-rays are 1488.2 eV, 1498.4 eV, 1509.4 eV, 1522.4 eV and 1537.4 eV, respectively, and agree well (within $\pm$ 0.8 eV) with those measured by Jamison *et al* [16] with 31 MeV Br ions using ADP crystal with a 4-inch curved crystal spectrometer. Jamison *et al* [16] have observed up to five satellite lines of Al Kα. The relative intensity values of KαL^0, KαL^1, KαL^2, KαL^3 and KαL^4 were found to be 14.1%, 33.7%, 34.7%, 14.1% and 3.3%, respectively. These ratios are expected to be different for every collision system and hence was not compared with the values obtained in ref. [16] which deals with a much lower velocity collision. It is to be noted that, the probability of having only one vacancy in the K shell is much smaller than that with one vacancy in the L shell or two vacancies in the L shell since I(KαL^0)/I(KαL^1)$\sim$2/5 and I(KαL^0)/I(KαL^2)$\sim$2/5. The ratio of the double-to-single L-vacancy production cross-sections (simultaneous with the K-shell vacancy) would be a very sensitive test to the theoretical models which incorporates the electron–electron correlation in the double ionization.

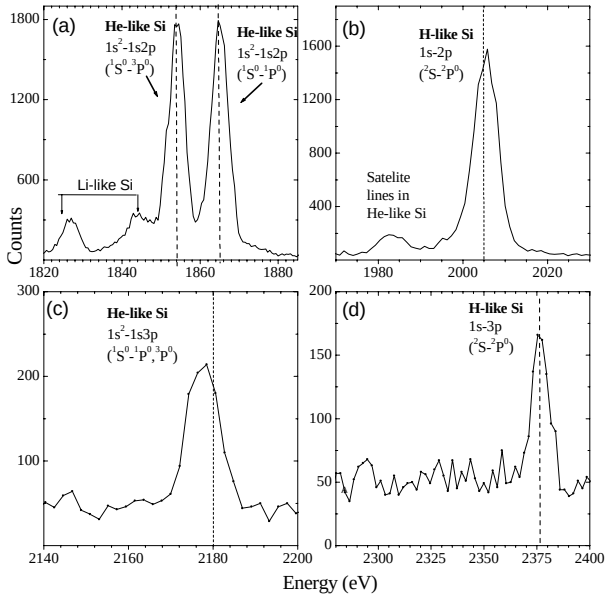

Figure 7. Projectile K X-ray spectrum for 80 MeV Si^{7+} in collisions with thin carbon foil. The transitions giving rise to the X-ray lines are indicated in the figure. The vertical dashed-lines represent the predictions of the theoretical model (see text).

5. Ionization of highly charged projectile ions

In another experiment, we used Si^{7+} ion beam with energy 80 MeV to collide with the C (about 20 $\mu g/cm^2$) target. The charge state 7+ is much lower with respect to the equilibrium charge state ∼12+ (at this energy) [17], one expect more probability of ionization than capture. The crystal makes 135° angle with respect to the incident beam direction. Since the X-ray source is moving (Si projectile), Doppler shift correction was made to identify the X-ray energy. The observed X-ray spectrum shows several peaks emitting due to the decay of H-, He- and Li-like Si ions (figure 7). The observed spectral lines were compared [18] with those calculated using the Breit–Pauli R-matrix method [19] and the relative atomic structure code SUPERSTRUCTURE [18,20]. The energy of measured X-ray lines are in good agreement with the theoretical values which are shown as vertical dashed-lines. The spectra were calibrated treating the H-(1s-2p/3p) as known and using the calculated values using theoretical model. Trabert *et al* [21] have measured the X-rays of various highly charged fast Si ions of energy 35–45 MeV by thin carbon foil which compares well with the present spectrum.

The area under the peaks, corrected for the intrinsic efficiency of the detector and divided by the fluorescence yield (ω) [22] is used to determine the approximate charge state distribution (q) of the projectile. We, therefore, observed 20.6%, 67.4% and 12% of H-like, He-like and Li-like Si ions, respectively, which approximately agrees [20] with the earlier studies. Ishihara *et al* [17] used magnetic spectrograph.

Therefore, the present measurement can be used for charge state distribution which will have importance for the accelerator technology. This is a new method to study the charge state distribution in contrast to the traditional technique of post-collision charge state analysis.

6. Conclusions

A crystal spectrometer has been reconditioned and developed to study the physics of ion–atom and electron–atom collisions. We have discussed all the necessary details of the spectrometer including LabVIEW-based automation and data acquisition. The spectrometer has been used to study the Kα satellite intensity of Al, the Mα and Mβ X-ray intensity of Au, and also Kα lines of Cl and K elements under keV energy electron impact. The Al–K X-ray satellite lines are studied under heavy-ion impact and it is shown that as large as four L-vacancies are created simultaneously with the K-vacancy, compared to only two satellites in case of electron-impact. This is the first time that one has observed the second satellite of Al in electron impact. In addition, the projectile X-ray lines arising from H-like, He-like and Li-like Si ions were detected and an approximate charge state distribution of the emerging ions was measured using this new technique. The design details along with the necessary information on the automation using LabVIEW has been provided. This control system is quite general and may find application in other equipments and detectors in different experimental setups.

Acknowledgment

We thank the Pelletron accelerator staff for smooth running of accelerator and TIFR central workshop. We also thank W A Fernandes and F A Rajgara for their help and useful discussions. We would like to thank A K Pradhan for providing theoretical values of X-ray transitions of Si ion.

References

[1] W L Bragg, *Proc. Cambridge Philos. Soc.* **17**, 43 (1913)
W H Bragg and W K Bragg, *Proc. R. Soc. London* **88**, 428 (1913)
[2] H H Johann, *Z. Phys.* **69**, 185 (1931)
[3] T Johansson, *Z. Phys.* **82**, 507 (1933)
[4] M Y Cauchios, *J. de Phys.* **3**, 320 (1932)
[5] J W M DuMond, *Rev. Scientific Instrum.* **18**, 626 (1947); *Ann. Phys. (Leipzig)* **17**, 716 (1933)
[6] S K Deshpande, S M Chaudhari, Ashok Pimpale, A S Nigavekar, S B Ogale and V G Bhide, *Pramana – J. Phys.* **37**, 373 (1991)
[7] C Bonnelle, P Jonnard, J M Andre, A Avila, D Laporte, H Ringuenet, M C Lepy, J Plagnard, L Ferreus and J C Protas, *Nucl. Instrum. Methods* **A516**, 594 (2004)
[8] Saint-Gobain Crystal and Detectors, Nemours Cedex, France (Website: http://www.crystals.saint-gobain.com)

[9] Website: http://xdb.lbl.gov
[10] J A Bearden, *Rev. Mod. Phys.* **31**, 78 (1967)
[11] F Bombarda, MIT-RLE report PTP 02/02 (Cambridge, MA 02139, 2002)
[12] Y Cauchios and C Bonnelle, *X-ray diffraction spectrometry: Atomic inner shell processes, Tome II: Experimental approaches and applications* edited by B Creasemann (Academic Press, 1975) pp. 84–121
[13] O Mauron and J Cl Dousse, *Phys. Rev.* **A66**, 042713 (2002)
[14] S Santra, A C Mandal, D Mitra, M Sarkar, D Bhattachrya and P Sen, *Nucl. Instrum. Methods* **B197**, 1 (2002)
[15] M Czarnota *et al*, *Rad. Phys. Chem.* **68**, 121 (2003)
[16] K A Jamison, C W Woods, R L Kauffman and P Richard, *Phys. Rev.* **A11**, 505 (1975)
[17] T Ishihara *et al*, *Nucl. Instrum. Methods* **204**, 235 (1982)
[18] A K Pradhan, private communication
[19] K A Berrington, W B Eissner and P H Norrington, *Comput. Phys. Commun.* **92**, 290 (1995)
[20] A Kumar *et al*, *Nucl. Instrum. Methods* **B248**, 247 (2006)
[21] E Trabert, I A Armour, S Bashkin, N A Jelly, R O'Brien and J D Silver, *J. Phys.* **B12**, 1665 (1979)
[22] E Behar and H Netzer, *Astrophys. J.* **570**, 165 (2002)